

NANOENGINEERED INJECTABLE HYDROGELS FOR ON-DEMAND AND  
LOCALIZED THERAPEUTIC DELIVERY

A Thesis

by

NIMA A. JALILI

Submitted to the Office of Graduate and Professional Studies of  
Texas A&M University  
in partial fulfillment of the requirements for the degree of

MASTER OF SCIENCE

Chair of Committee,	Akhilesh K. Gaharwar
Committee Members,	Daniel L. Alge
	Melissa A. Grunlan
Head of Department,	Anthony Guiseppi-Elie

August 2016

Major Subject: Biomedical Engineering

Copyright 2016 Nima A. Jalili

## ABSTRACT

“Smart” hydrogels are an emerging class of biomaterials that respond to multiple external stimuli and investigated for a range of biomedical applications, including therapeutic delivery, and regenerative engineering. Stimuli-responsive nanogels based on thermoresponsive polymers such as poly(N-isopropylacrylamide) (PNIPAM) and magnetic nanoparticles (MNPs), are developed as “smart carriers” for on-demand delivery of therapeutic biomolecules via magneto-thermal activation. However due to their small size and systemic introduction, these PNIPAM/MNPs nanogels result in limited control over long-term, localized therapeutic delivery.

Here, we developed an injectable nanoengineered hydrogel loaded with PNIPAM/MNPs for localize on-demand delivery of therapeutics (doxorubicin (DOX)). We have engineered shear-thinning and self-recoverable hydrogels by modulating crosslinking density of our methacrylated gelatin (GelMA) network. PNIPAM/MNPs nanogels loaded with DOX were entrapped within the GelMA pre-polymer solution prior to crosslinking. The temperature and magnetic field dependent release of loaded DOX was observed from the nanoengineered hydrogels (GelMA/(PNIPAM/MNPs)). The *in vitro* efficacy of DOX released from injectable nanoengineered hydrogels was investigated using preosteoblast and osteosarcoma cells. Overall, these results demonstrated that the injectable nanoengineered hydrogels can be used for on-demand and localized therapeutic delivery for biomedical applications.

## ACKNOWLEDGEMENTS

I would like to thank my research advisor and committee chair, Dr. Gaharwar for the countless hours of professional advising and helping me achieve my research goals. I learned many lessons from him including how to market the impact of my research to others. Because of this skill, I could make my friends and even strangers more interested in how great of a potential my project had on the future of biomedical research. I would also like to thank the rest of my committee (Dr. Alge and Dr. Grunlan) for their guidance and support throughout the course of this project. They helped me to always think about the clinical significance of every experiment I ran to prove the benefits of my nanoengineered construct, as well as help me prepare for my defense presentation.

Thanks also go to my friends and colleagues and the department faculty and staff for making my time in graduate school at Texas A&M University a great experience. When I accepted my position as a Master student in the Gaharwar Laboratory, I was unsure about balancing work and research with my personal life, but understanding friends as well as helpful labmates (specifically Jake Carrow, Lauren Cross, and C.W. Peak) made it possible.

I would also like to thank Janet Xavier and Dr. Jaiswal for their assistance in educating me in the various protocols I required to complete this project. In line with this, thanks to Madyson Muscarello, Pournima Prabhakaran, and Roshni Nambiar for assistance in data collection. Also, thanks to Ceylan Hayrettin and Dr. Ibrahim Karaman

for assistance in using their induction heating system for magnetic field experiments. And finally, Dr. Anup Bandyopadhyay for assistance in collecting SQUID data.

Finally, thanks to my family for all of the support they gave me through my five years in College Station. I cannot emphasize enough how none of this would have been possible without their help. Because of them, I learned the important lessons of knowing what I want and knowing what it takes to achieve those goals. My ‘efficient’ phone calls to my mom and dad while commuting from work to home were often the highlights of my day. I would also like to thank my sister, Emma, for having the patience of a saint. While I was swamped with experiments or coursework, she respected my space even though she was greatly missing me. It is crazy to think about how much she has changed in the last 5 years, but how our relationship has remained strong. Also, although I wish my dog Socks was by my side throughout this journey, every time I visited home or my family visited me, I knew that I was missed by the number of times he tackled me to the ground. I can’t wait to spend more time with him and the rest of my family now that my graduate career is over!

## NOMENCLATURE

AM	Acrylamide
AMF	Alternating Magnetic Field
DOX	Doxorubicin
EE	Encapsulation Efficiency
GelMA	Methacrylated Gelatin
LCST	Lower Critical Solubility Temperature
MNPs	Magnetic Nanoparticles
MRI	Magnetic Resonance Imaging
Nanocomposite	PNIPAM-co-AM/MNPs fixated in a GelMA matrix
Nanogels	PNIPAM-co-AM nanoparticles with MNP cores
OS	Osteosarcoma
PBS	Phosphate Buffered Saline
PNIPAM	poly(N-Isopropylacrylamide)
VPTT	Volume Phase Transition Temperature

## TABLE OF CONTENTS

	Page
ABSTRACT .....	ii
ACKNOWLEDGEMENTS .....	iii
NOMENCLATURE .....	v
TABLE OF CONTENTS .....	vi
LIST OF FIGURES .....	viii
LIST OF TABLES .....	ix
I. INTRODUCTION AND LITERATURE REVIEW .....	1
I.1 Magnetic Nanoparticles Used in Nanocomposites for Biomedical Applications .....	3
I.2 Thermoresponsive Polymers Used in Magnetically-Responsive Nanocomposites for Biomedical Applications.....	5
I.3 Magnetically Triggered Nanocomposite Hydrogels for Drug Delivery .....	7
II. MATERIALS AND METHODS .....	13
II.1 Materials .....	13
II.2 Synthesis of MNPs and Nanogels .....	13
II.3 Characterization of Nanogels .....	14
II.4 Synthesis of Gelatin Methacrylate.....	15
II.5 Preparation of Nanocomposite Hydrogels.....	15
II.6 Rheological Studies .....	16
II.7 Encapsulation of DOX in Nanogels and Release .....	16
II.8 2D Cell Exposure.....	18
III. RESULTS AND DISCUSSION .....	21
III.1 Characterization of MNPs and Nanogels .....	21
III.2 Rheological Studies.....	25
III.3 Release from Nanogels.....	29
III.4 2D Cell Viability .....	36
IV. CONCLUSIONS.....	40

REFERENCES.....43

## LIST OF FIGURES

	Page
Figure 1 Schematic of our nanoengineered injectable hydrogel .....	12
Figure 2 Hysteresis loop.....	22
Figure 3 MNP and nanogel characterization results.....	24
Figure 4 Rheological experiments.....	28
Figure 5 Preformed vs injected gel rheology .....	29
Figure 6 Plate reader calibration curves for DOX .....	31
Figure 7 Encapsulation efficiency results .....	32
Figure 8 Release studies on nanogels and nanocomposites .....	34
Figure 9 1 hour release comparison .....	36
Figure 10 MOS-J IC-50 plot .....	37
Figure 11 Mouse osteosarcoma (MOS-J) cell line exposure studies .....	38
Figure 12 Mouse preosteoblast (MC3T3) cell line exposure studies.....	38
Figure 13 DOX-loaded nanogel comparison .....	39



## LIST OF TABLES

	Page
Table 1: Summary of Common Magnetic Nanoparticles Used in Magnetically-Responsive Nanocomposites for Biomedical Applications.....	5
Table 2: Summary of Common Thermoresponsive Polymers Used in Magnetically-Responsive Nanocomposites for Biomedical Applications.....	7

## I. INTRODUCTION AND LITERATURE REVIEW

Osteosarcoma (OS), is a type of cancer that causes tumors in bone tissue that, like most cancers, can metastasize and severely increase mortality rates. OS mainly affects adolescents and teens. The 5-year survival rate changes from 60% to 15% if the tumor metastasizes. [1] The standard course of treatment for patients suffering from OS, like many types of cancer, includes surgical intervention to remove the tumor and aggressive chemotherapeutic or radiation treatment plans. Most of these current therapies may only delay the progression of tumor growth, and the effect of these treatments falls short of a cure, resulting in limited management without eliminating the disease. During surgical intervention, there is no guarantee that all tumor cells have been removed and such invasive procedures could expose tumor cells into circulation thus forcing a metastasis to occur.

In addition to a complex treatment plan, surgery and chemotherapy is expensive. Time at chemo clinics as well as paying for chemotherapeutics and catheter devices are costly. Just the office visits alone to chemotherapy and radiation therapy cost an average of \$30,000 per therapy. A range of therapies including use of ultrasound, gene delivery, and macromolecules is currently proposed for OS to improve upon the standard. Unfortunately, none of these therapies have translated into a new standard for clinical practice. Many research groups have utilized the chemotherapeutic drug Doxorubicin (DOX) as a model drug in drug delivery for cancer treatment. DOX has been shown to intercalate with DNA and trigger activation of cytotoxic pathways such as the Bcl-2/Bax

apoptosis pathway. [2] Local delivery of DOX is crucial for optimal cancer treatment. Typical chemotherapeutic treatment is systemic and has many potential side effects such as heart damage, nerve damage, bleeding urine, infertility, and liver and kidney damage. Systemic chemo also relies upon the fact that tumors have leaky vasculature that will allow for the majority of the drug to affect the tumor sites. Therefore, there is a critical need to develop effective therapies to locally deliver DOX in a controlled and triggered manner to prevent tumor regrowth and other side effects that can occur with standard clinical treatments.

Stimuli-responsive hydrogels can be designed to respond to external stimuli such as changes in temperature, pH, light, and ultrasound.[3-7] Hydrogels that experience physio-chemical changes due to external stimuli have great potential in the field of non-invasive and remote controlled therapies. [7] However, the use of these external stimuli (temperature, pH, light, and ultrasound) limits the applications of these responsive hydrogels systems to specific tissue regions. For example, thermo-responsive hydrogels can be used for skin-deep penetration, where external heating can be applied, while pH-responsive hydrogels can be used in tissue with specific pH ranges. Hydrogels responding to ultrasound waves and near-IR radiations have limited penetration ability due to high diffraction and absorption ability of tissues. To engineer a versatile stimuli-responsive system, nanoparticles that can generate stimuli to control the response of polymeric network are designed. These “smart hydrogels” are an emerging class of biomaterials that respond to multiple external stimuli and are investigated for a range of biomedical applications, including therapeutic delivery, bioimaging and regenerative engineering.

Magnetic nanoparticles (MNPs) responding to alternating magnetic fields (AMF) have been shown to generate heat due to its superparamagnetic nature. Due to this characteristic, MNPs are extensively used as magnetic contrast agents to improve imaging resolution for magnetic resonance imaging (MRI) as well as hyperthermia treatments.[8-10] By combining these MNPs with thermoresponsive polymers, a safe, deep-tissue response can be elicited to control the material behavior. These magneto-thermo responsive nanomaterials can be designed for “on-demand” therapeutics delivery and MRI sensing. Such responsive materials are sometimes utilized for systemic treatment of cancer by delivery to tumor sites through leaky vasculature, while others can be made as a controllable, biocompatible fixative to maintain long-term resolution of MRI scanning. [11, 12]

### **I.1 Magnetic Nanoparticles Used in Nanocomposites for Biomedical Applications**

Among different types of MNPs, ferromagnetic and superparamagnetic nanoparticles (**Table 1**) are extensively investigated for biomedical applications. [10, 13-17] Most often superparamagnetic MNPs are less than 30 nm in diameter. [18] Under alternating magnetic fields, superparamagnetic MNPs produces heat due to Brownian and Néel relaxation hyperthermia and occurs whenever the magnetic moment in the cores of SPM particles changes direction with high frequency. Brownian relaxation occurs in addition to Neel relaxation and is caused from movement of the entire SPM particle. For these relaxation mechanisms to occur, the particles must be superparamagnetic and single domain and therefore less than 30 nm. This hyperthermic potential is utilized for ablative

applications on tissue sites of interest. [8] Aggregation, corrosion, and loss of magnetism occur over time with magnetic nanoparticles. [9] In order for ferrous nanoparticles to stay in solution for a long period of time, synthesis usually includes a step for functionalizing each nanoparticle with molecules such as PEG, citric acid, oleic acid, or other molecules. [19]

Magnetite and hematite are the most commonly utilized ferromagnetic nanoparticles for biomedical applications due to their biocompatibility, potential for stability, and high magnetization ability. Magnetite, which has the chemical formula  $\text{Fe}_3\text{O}_4$  and may also be written as  $\text{Fe}_2\text{O}_3 \cdot \text{FeO}$ , contains  $\text{Fe}^{3+}$  as well as  $\text{Fe}^{2+}$  ions ordered unequally, which gives rise to a net magnetization ability. This high magnetization caused by its ferromagnetic and superparamagnetic capabilities makes it a great material for magnetic hyperthermia. Magnetite is commonly utilized in research as an MRI agent, hyperthermic agent, component in drug delivery constructs, as well as for scaffold-free tissue culture. [9, 19-21] Hematite has the formula  $\text{Fe}_2\text{O}_3$  and has been recently functionalized with fullerenes such as  $\text{C}_{60}$  for potential use in drug delivery, non-viral gene delivery, and MRI contrast mediums. [22-24]  $\gamma\text{-Fe}_2\text{O}_3$  is not as magnetically responsive as magnetite so in literature it is often incorporated into magnetic alloys such as the fullerene example. Another iron-containing nanoparticle used in biomedical application is FePt. FePt's ability to be surface modified like magnetite and hematite allows for various applications such as targeted drug delivery, photochemical therapy, biosensing, and imaging. [15, 25, 26] Finally, CoFe containing nanoparticles are also researched and have relevance in bioimaging and drug delivery applications. [13, 27, 28] Superparamagnetic

iron-containing nanoparticles such as these are utilized in many biomedical applications and have potential to become part of new clinical standards due to its lack of a significant difference in cell toxicity with varying concentrations. [29, 30]

**Table 1: Summary of Common Magnetic Nanoparticles Used in Magnetically-Responsive Nanocomposites for Biomedical Applications**

<b>Material (# Papers as of 3/2016)</b>	<b>Magnetic Behavior Utilized</b>	<b>Common Biomedical Applications</b>
Fe <sub>3</sub> O <sub>4</sub> (Magnetite) (1,004)	ferromagnetic, superparamagnetic	MRI contrast mediums, hyperthermic agents, drug delivery, cell migration
γ-Fe <sub>2</sub> O <sub>3</sub> (Hematite) (227)	ferromagnetic, superparamagnetic	MRI contrast mediums, drug delivery
FePt (88)	ferromagnetic, superparamagnetic	Photothermal cancer treatment, hyperthermic agents, cell migration
CoFe (24)	ferromagnetic, superparamagnetic	MRI contrast mediums, drug delivery

## **I.2 Thermoresponsive Polymers Used in Magnetically-Responsive Nanocomposites for Biomedical Applications**

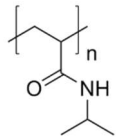
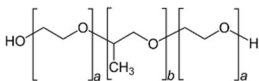
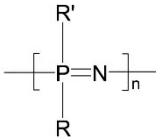
Thermoresponsive hydrogels are found in either hydrophilic or hydrophobic states dependent upon temperature. It is these types of polymers that are used to fabricate magnetically responsive hydrogels. By using factors such as the Neel and Brownian relaxation mechanisms discussed above, magnetic nanoparticles suspended or encapsulated by thermoresponsive hydrogels can act as local sources of heat to cause the thermal response. When activation of these magnetic nanoparticles ceases, the creation of

heat ceases and temperature returns to the ambient temperature surrounding the polymer. In this way, the reversibility of thermoresponsive hydrogels can be controlled with magnetic fields instead of with heating elements. Because of thermoregulation in human bodies, any transition temperature outside of a narrow range within body temperature (37 C) would require a clinician to cause patients to go under hypothermia or hyperthermia, which has potential for organ failure and other complications. When utilizing nanosized materials, temperature increases that occur locally would not cause these pathological temperature conditions. Therefore, a secondary response that allows localized, controlled increase in temperature in nanosized medical applications is highly researched. Various polymers with these properties have been utilized for biomedical purposes and are summarized in Table 2.

One such polymer, poly(N-isopropylacrylamide) (PNIPAM), is heavily researched for thermoresponsive applications. [7, 31-35] Common applications of to this polymer include drug delivery, cell sheet engineering, tissue engineered scaffolds, and DNA sensing. [36-41] Poloxamer is the generic name for tri-block copolymers consisting of two blocks of poly(ethylene oxide) (PEO) with a block of poly(propylene oxide) (PPO) in between. PEO's biocompatibility and shielding from protein adhesion are well researched due to the highly hydrophilic nature of this polymer. [42, 43] Poloxamers are sold commercially as Pluronics® by the chemical manufacturing company BASF. Poly(organophosphazene) (PPZN) is a family of macromolecules first isolated in the 1960s and are found to exhibit a reversible sol-gel transition with a change in temperature.

More recently, there have been biocompatible versions that can exhibit this change in a physiological temperature range. [28, 44]

**Table 2: Summary of Common Thermoresponsive Polymers Used in Magnetically-Responsive Nanocomposites for Biomedical Applications**

Material (# Papers as of 3/2016)	Chemical Structure	Thermal Transition Behavior	Common Biomedical Applications
PNIPAM (28,729)		LCST/VPTT	Drug delivery, cell sheet engineering
Ploxamer (54)		CMT	Drug delivery, cancer therapy, surfactants for other syntheses
Poly(organo-phosphazene) (12)	Varies; 	LCST/VPTT	Tissue engineered scaffolds, in situ gelation, drug delivery, long term MRI contrast agent

### I.3 Magnetically Triggered Nanocomposite Hydrogels for Drug Delivery

Researchers utilize nanocomposites for controlled drug delivery for combating drug uptake issues, optimizing time within the therapeutic threshold, as well as enhancing biocompatibility of healthy tissues. Many drugs are water insoluble, have too fast of a half-life, and can cause potentially serious side-effects. All pharmaceuticals require the correct dosage to maintain a therapeutic threshold. Many analgesics utilize delayed release or diffusion kinetics to properly deliver drugs within this threshold, but are systemic in



nature and typically have to get above the threshold into slightly toxic conditions to allow for diffusion out of the system and stay in the therapeutic range for a longer amount of time. This is partially responsible for many pharmaceuticals' harmful side effects. Also, having a drug delivery vehicle small enough to enter into tissue is beneficial for increasing uptake and getting the drug payload to the tissue sites of interest, as seen in smaller molecules that exist systemically. Biocompatibility is another issue that limits options for the application of drug delivery. Having a controlled system requires no interference from the immune system. When applying nanocomposite systems for drug delivery or other applications, interference from the immune system will cause digestion of the construct by macrophages and cause either burst release or prevent release by fibrous encapsulation that covers foreign bodies too large to be uptaken in layers of fibroblasts which close it off from the rest of the body. In this section, we explore ways that researchers have overcome these limitations with the addition of two or more components to the magnetic nanoparticles.

In recent years, Jaiswal *et al.* synthesized  $\text{Fe}_3\text{O}_4$  nanoparticles conjugated with either poly(ethylene glycol) (PEG) or polyhedral oligomeric silsesquixone (POSS). [45] These particles were then encapsulated by copolymerizing a layer of PNIPAM to produce a nanocomposite hydrogel system for *in vitro* release of incorporated Doxorubicin with and without presence of an AMF field. At temperatures above the material's intrinsic volume phase transition temperature (VPTT), the PNIPAM expels its water content to form globules and precipitates out of solution. This occurs because hydrophobic constituents (isopropyl) of the polymers forming the hydrogel become entropically-

favored over the hydrogen bonding from hydrophilic components, resulting in thermally induced conformational changes. PNIPAM has its VPTT at 33-35 C, and in order to increase or decrease the transition temperature it can be copolymerized with hydrophilic or hydrophobic polymers, respectively. The process of hydrophilic to hydrophobic transition at VPTT is reversible, which enables its usage in carrying and releasing aqueous soluble therapeutics as a controlled drug delivery system. These nanocomposites were around 200 nm in size and relatively spherical. This three component system exhibited VPTT behavior at around 40 C which allowed for controllable release of encapsulated cargo to occur from magnetic hyperthermia alone instead of burst release once exposed to body temperature. Different incubation times of the nanocomposites with their tested HeLa cell line, as well as different AMF exposure times were explored to discover optimal release percentage of encapsulated DOX. It was seen that a 48 hour incubation period after 1 hour of magnetic field exposure allowed for the highest release at close to 40% or 10 $\mu$ g of DOX. This level of release allowed for a significant decrease in cell viability by close to 80%, which is expected with DOX exposure to a cancer cell line. Jaiswal also noted that no macroscopic temperature change was exhibited from the samples during RF exposure, which is beneficial for preventing unwanted tissue ablation.

With a low mortality rate, when an OS tumor is found, surgery is a standard option for treatment. However, like all surgeries, there are always risks involved. A potential risk that can occur in that during tumor excision, some cells can venture elsewhere in the body and develop other tumors. [46] Therefore, a current standard is for intravenous injection of chemotherapeutics or radiation therapy to be the sole or secondary source of treatment.

It is well researched that tumor sites typically have ‘leaky’ vasculature, or vasculature that allows for easier movement into the surrounding interstitial tissue space. [47-50] Make use of this knowledge, intravenous approaches statistically should have a greater chance of affecting tumor sites than healthy interstitial tissue.

However, a common problem occurs with free-roaming nanocomposites in vasculature or free tissue space due to the reticuloendothelial system. [11, 29, 51] This system involves phagocytic immune cells located in connective tissue throughout the body. By having nanosized particles with loaded-therapeutics that are able to be uptaken so readily by cells, these phagocytic cells also uptake them and prevent delivery to the desired tissue site. In addition to this prevention, if loaded with chemotherapeutics, such phagocytic cells as the Kupffer cells in the liver, pulmonary alveolar macrophages in the lungs, and glomerular mesangial cells in the kidneys all would entrap these cytotoxic drugs in healthy tissue sites and could cause cell death of non-tumor cells. It was therefore a concern for us to maintain spatial control in addition to temporal control of delivery of therapeutics.

Gelatin is a natural polymer made of denatured collagen. Found in many food products, this material has applications in the biomedical field due to its injectability and ability to mimic extracellular matrices. This material has been utilized for injectability potential for several biomedical applications including a vessel for wound healing. [52] By methacrylating gelatin, researchers have created a stronger, crosslinked gel that can be incorporated with nanoparticles for various biomedical purposes. Methacrylated gelatin has also been shown to be injectable and maintain RGD binding sequences to assist in cell

adhesion. [53-56] Therefore, addition of gelatin-based hydrogels allow for fixity for nanoparticles as well as promoting cell attachment from cells at desired tissue sites to facilitate therapeutic delivery.

A widely popular thermo-responsive polymeric hydrogel poly(*N*-isopropylacrylamide) was copolymerized with acrylamide and employed for this application due to its biocompatibility and stimuli-responsive nature [57]. By coating the MNPs with this thermoresponsive polymer shell, a nanogel drug reservoir with controllable release was made. The incorporation of MNPs allow for magnetic hyperthermia to heat surrounding stimuli-responsive material. Utilizing methacrylated gelatin allowed the construct to gain the spatial control we desired and reduced chances of drug-loaded nanocomposites from leaving the targeted tissue site. The nanogels were encased in photo-polymerizable gelatin matrix (namely gelatin methacrylate or GelMA) and injectability was proven possible as well as maintained viability of different cell types. Therefore, we offer a biocompatible, minimally-invasive tool where the use of external alternating magnetic fields remotely can induce the release of loaded drug in a controlled fashion. A schematic illustrating our construct can be seen in **Figure 1**.

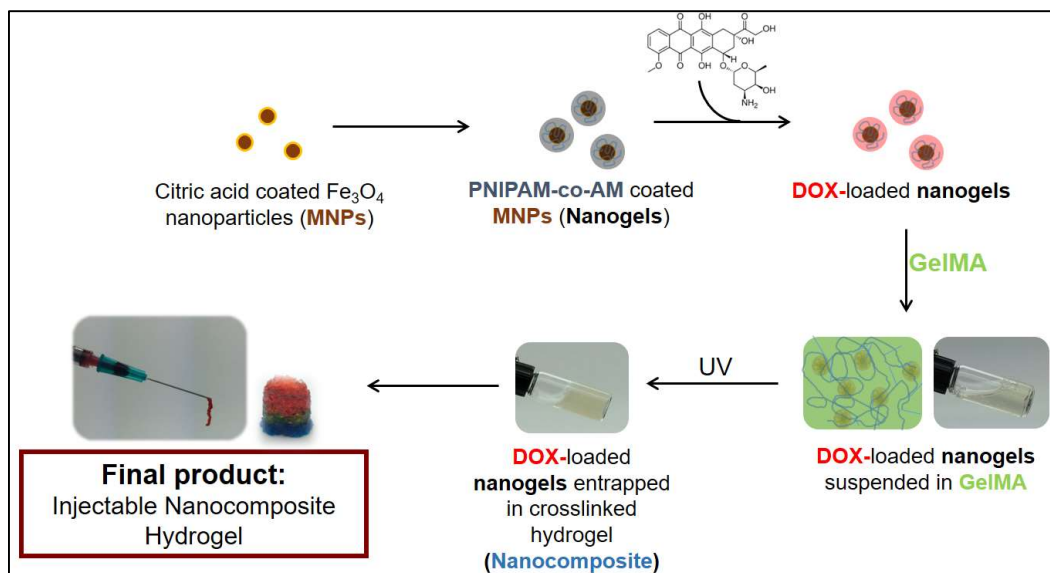


**Figure 1 - Schematic of our nanoengineered injectable hydrogel**

## II. MATERIALS AND METHODS

### II.1 Materials

Ammonium hydroxide solution ( $\text{NH}_4\text{OH}$ , ACS reagent, 28-30%  $\text{NH}_3$  basis), ammonium persulfate (APS, ACS reagent, 98+%), citric acid (99%), ferric chloride hexahydrate ( $\text{FeCl}_3 \cdot 6\text{H}_2\text{O}$ , ACS reagent, 97%), ferric chloride tetrahydrate ( $\text{FeCl}_2 \cdot 4\text{H}_2\text{O}$ , ReagentPlus®, 98%), gelatin from porcine skin (gel strength 300, Type A), N,N'-Methylenebis(acrylamide) (BIS, 99%), N-isopropylacrylamide (NIPAM, 97%), and sodium metabisulfite (SBS, 99+%) were all purchased from Sigma-Aldrich. Doxorubicin.HCl (DOX, 98%) was purchased from Cayman Chemical. Acrylamide (AM, 98+%) was purchased from Alfa Aesar. Sodium dodecyl sulfate (SDS, Biotechnology grade) was purchased from Amresco. Lithium acylphosphinate (LAP) photoinitiator was kindly provided by Dr. Daniel Alge's laboratory at Texas A&M University (College Station, TX). All chemicals were used as received without further purification or processing. Megaohm water ( $17.8 \text{ M}\Omega \cdot \text{cm}$ ) was used for all experiments.

### II.2 Synthesis of MNPs and Nanogels

Citric acid coated MNPs were synthesized via co-precipitation method as described previously. [58] In short,  $\text{FeCl}_3 \cdot 6\text{H}_2\text{O}$  and  $\text{FeCl}_2 \cdot 4\text{H}_2\text{O}$  solutions were mixed together and  $\text{N}_2$  purged for 30 minutes. An oil bath was heated to 70 C for 30 minutes and then a solution of  $\text{NH}_4\text{OH}$  was added dropwise and a black precipitate was formed immediately. After 30 minutes, a solution of citric acid was added and the temperature

was increased to 90 C and left for 1 hour. The MNP solution was left to cool to RT and magnetically separated from the solution for washing 5 times with DI H<sub>2</sub>O. The concentration of the washed solution was determined by measuring iron content in the resultant product using ion coupled plasma atomic emission spectroscopy (ICP-AES). Their magnetization ability was measured via superconducting quantum interference device (SQUID).

These MNPs were then embedded within poly(N-isopropylacrylamide-co-acrylamide) (PNIPAM-co-AM) via free radical polymerization method described elsewhere to make PNIPAM-co-AM/MNPs (nanogels). [45, 59] A solution of NIPAM, AM and MNPs for nanogels synthesis) were added to the flask and stirred and N<sub>2</sub> purged for 30 minutes. BIS and SDS solutions were each added dropwise to the flask and purged for another 30 minutes. Then the oil bath was heated to 70 C and APS and SBS solutions were each added dropwise. The reaction was allowed to continue for 5 hours and returned to room temperature. In order to isolate nanogels, magnetic separation overnight was performed. The solution was then freeze-dried for storage.

### **II.3 Characterization of Nanogels**

Hydrodynamic particle size, VPTT determination, and zeta potential were performed with a Zetasizer Nano ZS (Malvern Instruments, UK). ATR-FTIR measurement was performed with an FTIR spectrometer (ALPHA, Bruker, USA) and samples were of air-dried MNPs, NIPAM, AM, lyophilized PNIPAM-co-AM, and lyophilized nanogels. To view particle shape and confirmation of a presence of an MNP

core in the nanogels, TEM was performed on MNPs and nanogels (JEM-2010, JEOL, JP). Nanogels were also imaged with SEM (JSM-7500F, JEOL, JP). TGA measurement was performed with a TGA Q50 (TA Instruments, DE) to confirm copolymerization ratio and weight percentage of MNPs in nanogels.

#### **II.4 Synthesis of Gelatin Methacrylate**

Gelatin methacrylate with a methacrylation degree of 80% was synthesized as discussed previously. [54] The final solution of 80% methacrylated gelatin methacrylate (GelMA) was dialyzed for 7 days, filtered with quantitative filter paper and then freeze-dried for storage purposes. Lyophilized GelMA was rehydrated in a 2.2 mM LAP solution. LAP was chosen as the photoinitiator due to problems with photobleaching of DOX when we utilized more common photoinitiators such as Irgacure® 2959. [60] A UV light source (Omnicure S2000, Lumen Dynamics, Canada) set to an intensity of 10 mW/cm<sup>2</sup> was used for gel crosslinking.

#### **II.5 Preparation of Nanocomposite Hydrogels**

Water-swollen nanogels were entrapped within a gel for rheological studies. 5 mg of nanogels were suspended in 1 mL of GelMA and UV crosslinked. To perform stress, frequency, and shear stress sweeps, a 1 mm thick sheet was crosslinked in a sandwich mold and 7 mm diameter punches were made. In addition to this, extruded gels of 1 mL of gel from a syringe with an 18G needle were tested for comparison with stress and frequency sweeps. The extruded gels were also tested for cyclic recoverability after high



shear (100%). 5 mg of drug-loaded nanogels were well-dispersed and entrapped within a UV-crosslinked gel for release experiments. In order to make nanogels dispersed in the gel, the pellet of washed DOX-loaded nanogels was re-suspended and vortexed within a 100  $\mu$ L solution of GelMA + LAP, after which the nanocomposite precursor was exposed to UV light.

## **II.6 Rheological Studies**

Shear stress and frequency sweeps were completed on an Anton Paar Physica MCR 301 rheometer (Anton-Paar GmbH, Austria). All experiments were completed at a physically relevant temperature (37 °C) using a humid atmosphere using a solvent trap. Shear rate sweeps were performed from 0.1-100 1/s to determine the injectable characteristics. The linear visco-elastic region of the samples were determined via a frequency sweep executed at 1 Pa between 0.1-100 Hz. Shear stress sweep was performed at 1 Hz between 0.0-100 Pa. Frequency and shear stress sweeps were completed on circular sheets of sample as well as extruded samples.

## **II.7 Encapsulation of DOX in Nanogels and Release**

DOX absorbance and fluorescence was measured with an Infinite® 200 PRO microplate reader (Tecan, Switzerland). Various weights of lyophilized nanogels (2.5, 5, 10, and 15 mg) were re-suspended in 1 mL solutions of 100  $\mu$ g DOX to obtain optimal loading. In addition to this, 5 mg of lyophilized nanogels were also rehydrated in 1 mL solutions of varying concentrations of DOX (25, 50, 100, 150  $\mu$ g/mL). After overnight

swelling at 4 C, the nanogels were centrifuged and washed 4x with chilled DI H<sub>2</sub>O. The DOX concentration loaded within the nanogels was found via encapsulation efficiency (EE) calculations (Equation 1).

$$EE (\%) = \frac{\text{weight of feed cargo} - \text{weight of unloaded cargo}}{\text{weight of feed cargo}} * 100 \text{ (Equation 1)}$$

Weight of the unloaded cargo was found by measuring and summing fluorescence of the supernatant after each round of centrifugation.

To measure release of nanogels, 5 mg of 100 µg/mL loaded and washed nanogels were suspended in 1 mL of 1X PBS inside of a floating dialysis tube as sink-reservoir system using dialysis membrane (Mol. Wt. ~ 10,000 Da). 1 mL was taken at timepoints of various hours, and then refilled with 1 mL of 1X PBS after each timepoint. These experiments were done at 37 C and 50 C. Fluorescence was then measured using the microplate reader. Cumulative release was then calculated and plotted versus time.

An Ambrell® EasyHeat 2.4 kW induction heating system (Ambrell, UK) was utilized for generation of an AMF to be exposed to the nanocomposite system at RT. The usage of this generator was made possible with help from Dr. Ibrahim Karaman's laboratory at Texas A&M University. A 0.25 inch (0.635 cm) thick copper coil of 0.5 inch (1.27 cm) inner radius and 6 turns was utilized with a current of 400 A alternating at 170 kHz to produce a magnetic field of 2.99x10<sup>4</sup> A/m (0.0375 T). The magnetic strength required to produce a release from our system was calculated using the Biot-Savart Law (Equation 2),

$$H = \frac{Ni}{\sqrt{4R^2+L^2}} \text{ (Equation 2)}$$

where  $H$  is magnetic field strength in A/m,  $N$  is number of turns,  $i$  is the current in Amperes,  $R$  is the inner coil radius in meters,  $L$  is the coil length in meters. [61] A DOX-loaded nanocomposite 100  $\mu$ L droplet was submerged in 1 mL 1X PBS within an Eppendorf tube. A control tube was left at RT, while the other was exposed to the AMF. After 1 hour of exposure, sample and control tubes were centrifuged and the PBS solution was extracted and fluorescence measured in order to obtain amount of DOX released.

## II.8 2D Cell Exposure

Mouse preosteoblasts (MC3T3-E1 Subclone 4, ATCC) were cultured in normal growth media composed of  $\alpha$ -minimal essential media (AMEM, Hyclone), 16.5% fetal bovine serum (Atlanta Biologicals, USA), and 1% penicillin/streptomycin (100 U/100  $\mu$ g/mL, Gibco). Similarly, mouse osteosarcoma cells (RFP-MOS-J) were cultured in Dulbecco's modified eagle media (DMEM, Hyclone), 10% fetal bovine serum (Atlanta Biologicals, USA), and 1% penicillin/streptomycin (100 U/100  $\mu$ g/mL, Gibco). RFP-MOS-J cell line was kindly provided by Dr. Roland Kaunas' laboratory at Texas A&M University. Media was changed every 3-4 days and cells were passaged at ~70-80% confluency.

To test the cytotoxicity of doxorubicin, an MTT assay (MTT assay Kit) was performed with the RFP-MOS-J cell line. Cells were seeded at a density of 10,000 cells per well in a 96 well plate and allowed to proliferate for 24 hours. Cells were then treated with varying concentrations of DOX for 6 hours. After the 6 hour treatment, cells were washed with sterile 1X PBS (PBS, Corning) and incubated in normal growth media for 48

hours. Next, 100  $\mu$ L of fresh media was added to the samples along with 10  $\mu$ L of MTT reagent. The samples were then incubated at 37°C for 3 hours. After incubation, media and MTT reagent were removed and the resulting crystal was dissolved with a 100  $\mu$ L of a dimethyl sulfoxide (DMSO), isopropyl alcohol (IPA) solution (DMSO:IPA). The samples were well mixed and the absorbance was read at 540 nm. The IC50 curve for doxorubicin exposed to MOS-J cells was found through normalization. Similarly, suspensions of 5mg nanogels and DOX-loaded nanogels were exposed to the RFP MOS-J and MC3T3 cells for 6 hours and the cytotoxicity was determined using the same treatment procedure and MTT assay.

In addition, a Live/Dead assay was performed on both cell lines treated with solutions of DOX, the 5mg nanogels, and DOX-loaded nanogels. The Live/Dead reagent was prepared using ethidium homodimer and Calcein AM (Santa Cruz Biotechnology Inc, USA). After cells had been subjected to similar treatment conditions discussed above, they were washed with 1X PBS and incubated at 37°C with the Live/Dead reagent for 30 minutes. The samples were then washed with 1X PBS and an epifluorescence microscope (TE2000-S, Nikon, USA) was used to image.

Finally, the cytotoxicity of the nanocomposite was tested using the RFP MOS-J cells. Cells were seeded into a 24 well plate and allowed to adhere for 24 hours. To isolate the results of the study to show *in vitro* release behavior, transwell inserts were used instead of direct placement in wells in order to expose the cells to the GelMA matrix for 6 hours. After 6 hours the inserts were removed and cells were incubated for 48 hours

similar to the previous viability studies. Live/Dead and MTT assays were performed on the samples.

Uptake of DOX loaded nanogels after 6 hours in preosteoblasts was observed using an epifluorescence microscope (TE2000-S Nikon, USA). Prior to imaging, samples were fixed with 2% glutaraldehyde in 1X PBS for 20 minutes, treated with 0.1% Triton-X100 for 5 minutes at room temperature, then incubated with DAPI for 5 minutes at 37°C.

### III. RESULTS AND DISCUSSION

#### III.1 Characterization of MNPs and Nanogels

In order to identify our nanoparticle components within the nanocomposite system, we performed various characterization techniques. Low polydispersity was seen when we performed dynamic light scattering on our citric acid-capped  $\text{Fe}_3\text{O}_4$  magnetic nanoparticles (MNPs) as well as the PNIPAM-co-AM coated MNPs. This showed that we had very little aggregation issues, which was beneficial for good spread of suspension within our nanocomposite construct. In the graph shown in **Figure 3b**, two peaks were separately measured and overlaid to show the mean values of 28 nm and 255 nm diameters for MNPs and nanogels, respectively. Comparing the mean diameter of MNPs to the TEM of these MNPs shows that there was an initial aggregation of 5-10 nm MNPs. This behavior is shown in the TEM of the nanogel system where more than one MNP makes up the core of each nanogel and matches the size of the results from Dynamic Light Scattering (**Figure 3a**). We believe that this slight aggregation is due to the capping group of citric acid not being as stable as some other functionalizing agents such as oleylamine, which give monodisperse colloidal MNP solutions. [13] Although the sizing of this MNP core is close to the limit of SPM behavior, because each MNP is below the size of the aggregate, SPM behavior was expected to remain and was confirmed so by the hysteresis loop plotted from our SQUID results which showed a high magnetization of  $\sim 65$  emu/g (**Figure 2**).

DLS of the nanogels showed that the hydrodynamic diameter was low in polydispersity at a size of 255 nm (**Figure 3b**). This is within the range of similar nanogels synthesized by Jaiswal *et al* and other researchers, with many drug-loaded vessels at or less than 500 nm still able to be uptaken by cells. [45, 62, 63]

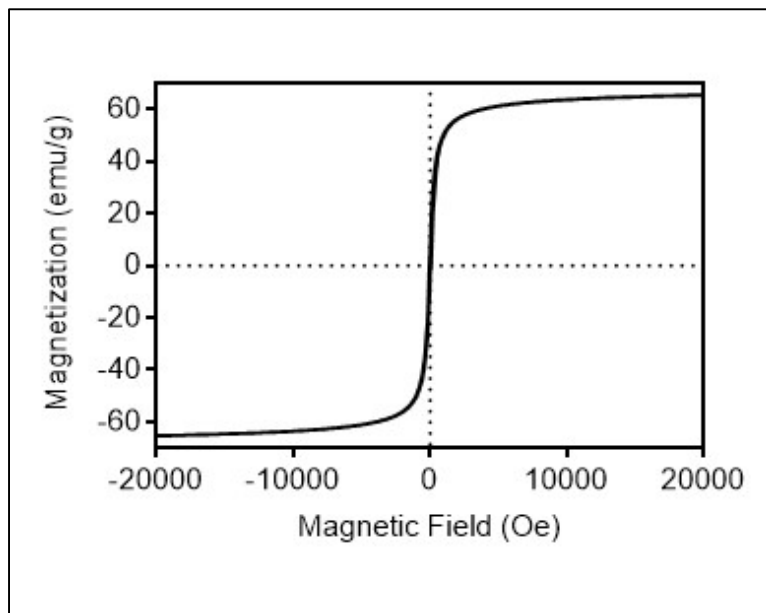


**Figure 2 – Hysteresis loop. SQUID showed high magnetization of 65 emu/g for our MNPs.**

A temperature sweep of the nanogels was run to discover the deswelling temperature of our nanogels (**Figure 3c**). As the VPTT was identified as occurring at 45 C, the size of particles begins to decrease at around 41 C. We opted to use VPTT versus the more commonly used LCST to describe this behavior because these are crosslinked polymer hydrogels, and because we determined transition temperature via DLS temperature trend versus a cloud point method or DSC. [64] By copolymerizing with a hydrophilic monomer, hydrogen-bonding interactions dominated more and required a

higher energy for hydrophobic interactions to dominate. These results are similar with the phase transition measured in Zhang *et al* for a similar copolymer ratio. [59] TGA in **Figure 3c** showed a copolymerization ratio of approximately 80:20 (NIPAM:AM) as desired to increase the VPTT. The weight of MNPs within the nanogel sample was approximately 15%. This decrease still occurs above normal body temperature (37 C), so we accepted the copolymer ratio and proceeded with experiments utilizing this nanogel synthesis.



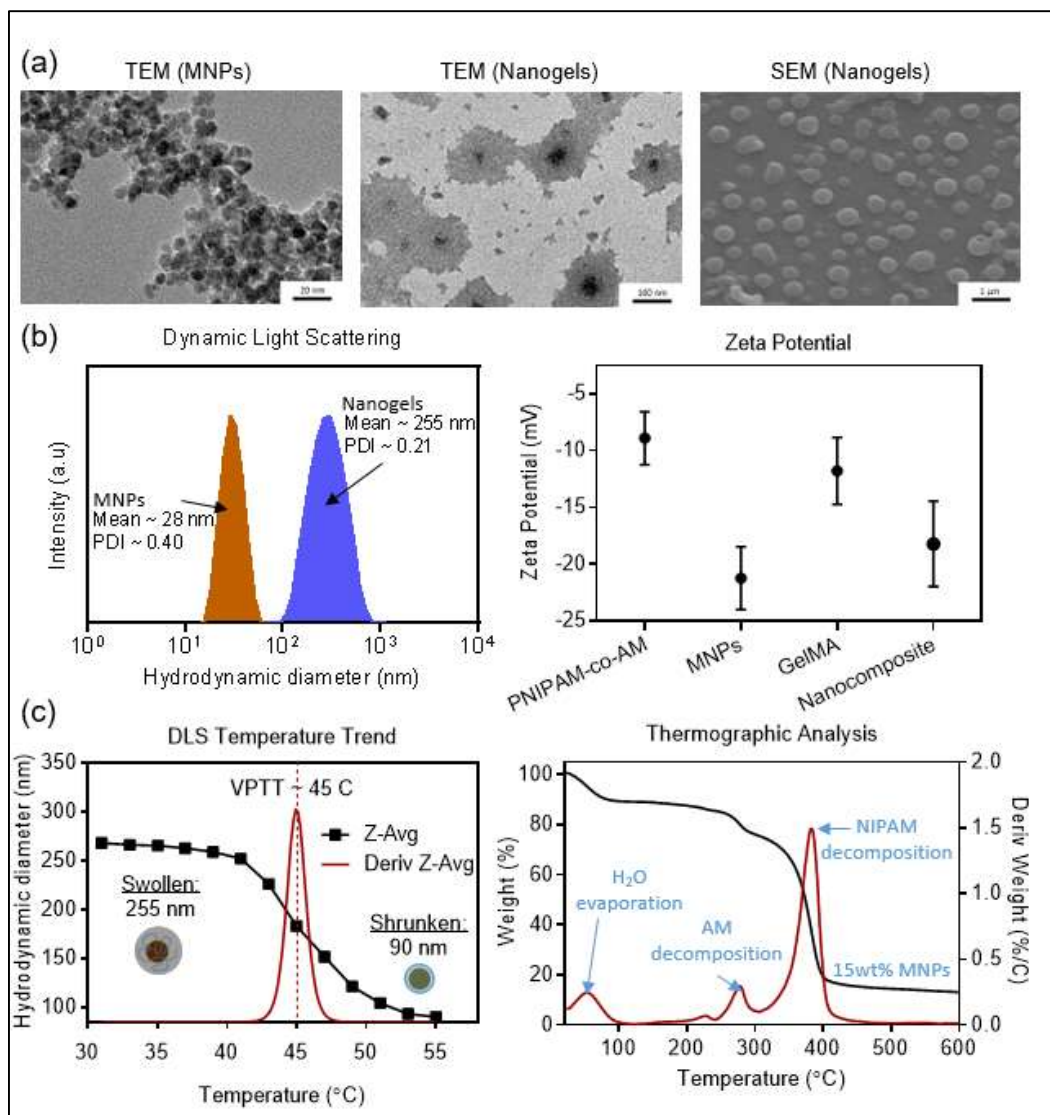


**Figure 3 - MNP and nanogel characterization results. (a) TEM and SEM of MNPs and nanogels. (b) DLS and Zeta Potential. MNPs had a mean of 28 nm with a PDI of 0.40 and nanogels were of a mean of 255 nm with a PDI of 0.21. The zeta potential of the nanocomposite showed a more negative z.p. than just GelMA. (c) VPTT was determined to be 45 C from a DLS temperature sweep and copolymer determination was approximately 80:20 (PNIPAM:AM) from TGA and it also showed an MNP wt% of 15%.**

### III.2 Rheological Studies

Using an injectable system requires characterization of its material behavior before and after injection into our tissue site of interest. In order to characterize the mechanical properties of our nanocomposite, rheological studies were performed on 5 wt% gels and gels with 5 mg nanogels added (nanocomposite). Frequency sweep between 0.1-10 Hz was performed on all samples, determining the linear visco-elastic region of the samples. There was a slight increase in the storage modulus with frequency  $> 5$  Hz which could be attributed to bond breakage within the GelMA backbone. Interestingly, we observed no difference between samples containing nanogels and those without regardless of concentration. Addition of nanoparticles into injectable hydrogel constructs has been investigated by researchers. [52, 65] When adding silica nanoparticles to gelatin, Gaharwar *et al.* observed an increase in storage moduli with higher nanoparticle content. This difference from what is seen in literature suggests that our nanogel amount in the nanocomposite is not high enough to make a significant difference in gel strength. Although there was no significant rheological difference shown between gels and nanocomposites, zeta potential confirmed nanogel presence in our nanocomposite due to a more negative zeta potential than just our methacrylated gelatin due to the negatively charged MNPs; therefore a considerable amount of nanogel was present in the nanocomposite (**Figure 3b**). Stress sweeps show similar results as frequency sweeps. In each, the plateau is approximately 200 Pa (**Figure 4 a, b**). Our data suggests that the small amount of nanogels and limitations due to physical entrapment within the GelMA led to limited changes in internal stress and therefore no pronounced mechanical variation.

PNIPAM has been well characterized rheologically by itself, though from our investigation we are one of the first to use it in such a fashion as a filler material. [66] The low storage modulus of our gel is recognized, but due to the high affinity of cell adhesion on gelatin hydrogels, we preferred a weaker substrate that would not cause proliferation of cancer cells after injecting our nanocomposites to tumor sites. [67]

Due to the end goal of being able to inject our material, we then investigated how the sample behaves under high shear to determine the yield stress of the material. When passing a material through a syringe needle during injection into tissue sites, a fluidic flow is achieved through introduction of high shear stress. For a solid, crosslinked gel like ours, we expected a return to a gel state from its more fluid flow. Shear rate sweeps from 0.1-100 1/s indicated that all samples are shear-thinning: the sample viscosity decreased with increasing shear rate (**Figure 4c**). Our data, both experimentally and in practice, suggest that the nanofiller has no effect on the ability to extrude material out of a needle. We further investigated recoverability of the sample via application of high shear rate and then no shear. Over 3 cycles, the sample recovers quickly to its pre-sheared storage modulus (**Figure 4d**). To be clinically relevant, thixotropic recoverability samples were crosslinked within a syringe and extruded at a rate of 2 mL/min. This ability to recover was comparable to thixotropic studies by Gaharwar *et al* when adding nanoparticles to gelatin matrices. [52] It is believed that the weakness of the gel as well as the temperature at which we kept our gels at during testing (37 C) were responsible for keeping our nanocomposite recoverable and preventing brittle fracture upon injection.

The rheological difference between preformed samples tested and extruded samples were also investigated (**Figure 5**). Comparing extruded and non-extruded samples, we found no difference in the recoverable behavior, leading to the injectable uses of this material. Due to the high shear on our crosslinked gel out of a syringe, we expected there might be some bond breakage due to forcing this preformed gel. However, no significant difference was shown in storage moduli between preformed and injected samples, so rheological studies from **Figure 4 a-c** of preformed gels are proposed to be relevant to the final nanoengineered construct. We anticipate that upon injection, the sample will remain within a localized area. Depending on the initial degree of crosslinking, UV light can be re-applied and the sample further covalently crosslinked.

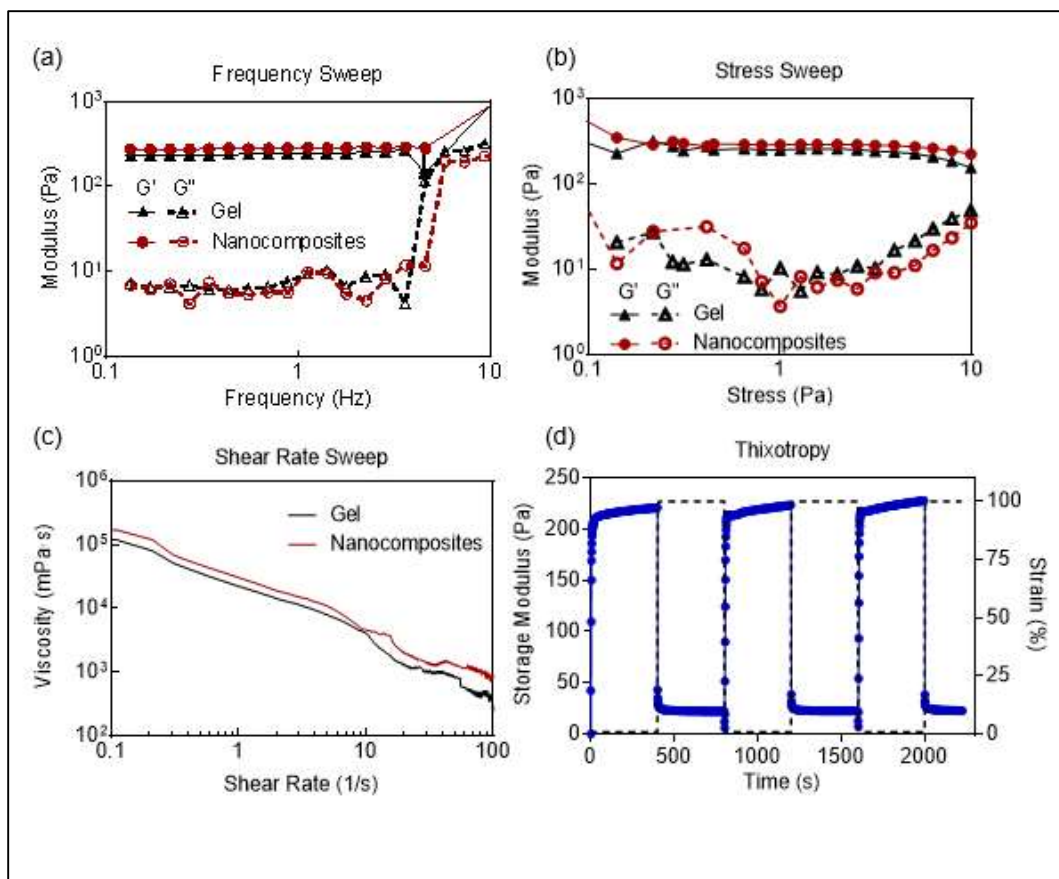


**Figure 4 - Rheological experiments. (a,b) Frequency and stress sweeps of 5 wt% gel (Gel) and 5 wt% gel with 5 mg nanogels added (Nanocomposites).  $G'$  is approximately 200 Pa and has no significant difference between Gel and Nanocomposites. (c) A shear rate sweep showed shear-thinning behavior for both Gel and Nanocomposites. (d) Injectability study on 5 wt% gel showed recoverability of original strength after 3 cycles.**

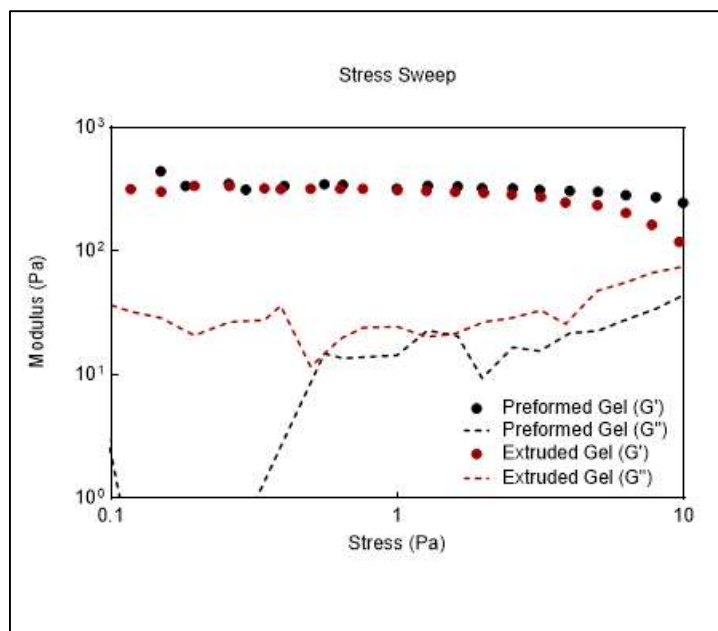


**Figure 5 – Preformed vs injected gel rheology. Stress sweep performed on equal volumes of preformed discs of 5 wt% gel and extruded strands of 5 wt% gel, with no statistical difference found.**

### III.3 Release from Nanogels

In order to observe release kinetics from our system with and without presence of stimuli, we performed thermal and magnetic release studies. First, in order to experimentally quantify release from our nanocomposites, calibration on our plate reader was performed with varying DOX concentrations within the range expected to be seen throughout our studies. The calibration and standard curves of DOX from our plate reader can be found in **Figure 6**. A highly linear trend allowed us to quantify DOX concentration from absorbance or fluorescence information. The weight of nanogels and DOX were used based from encapsulation efficiency studies shown in **Figure 7**. 5 mg nanogels rehydrated with 100  $\mu\text{g/mL}$  DOX showed to have the best loading content at  $42.1 \pm 8.1\%$  efficiency

(or  $42.1 \pm 8.1$   $\mu\text{g}$  loading), so all release studies were performed with these nanogel and DOX weights. This loading efficiency was similar to work shown by Shah *et al.* [68] We believe that this combination of nanogel and DOX concentration was best due to it having enough surface area available to load as much DOX as possible. With a Gaussian distribution profile, one-way ANOVA was performed followed by Tukey's multiple comparisons test. 100  $\mu\text{g}/\text{mL}$  within 5mg of nanogels showed the best encapsulation efficiency with significant difference ( $p < 0.05$ ) when comparing 50 and 150 to 100  $\mu\text{g}/\text{mL}$  DOX. We believe that this decrease after 100  $\mu\text{g}/\text{mL}$  was due to supersaturation of the DOX solution. When EE of 100  $\mu\text{g}/\text{mL}$  was tested, a significant difference between 2.5 and 5 mg as well as 5 mg and 15 mg nanogel weights was found ( $p < 0.01$  and  $p < 0.05$ , respectively). Above 5 mg, this decrease in encapsulation efficiency could be attributed to packing of the lyophilized nanogels, which would limit surface area available for uptake. Below 5 mg, we found the pellet of DOX-loaded nanogels to be too small to utilize this method of encapsulation study and that the concentrations tested were too saturated for the amount of nanogels to absorb a considerable amount of DOX.

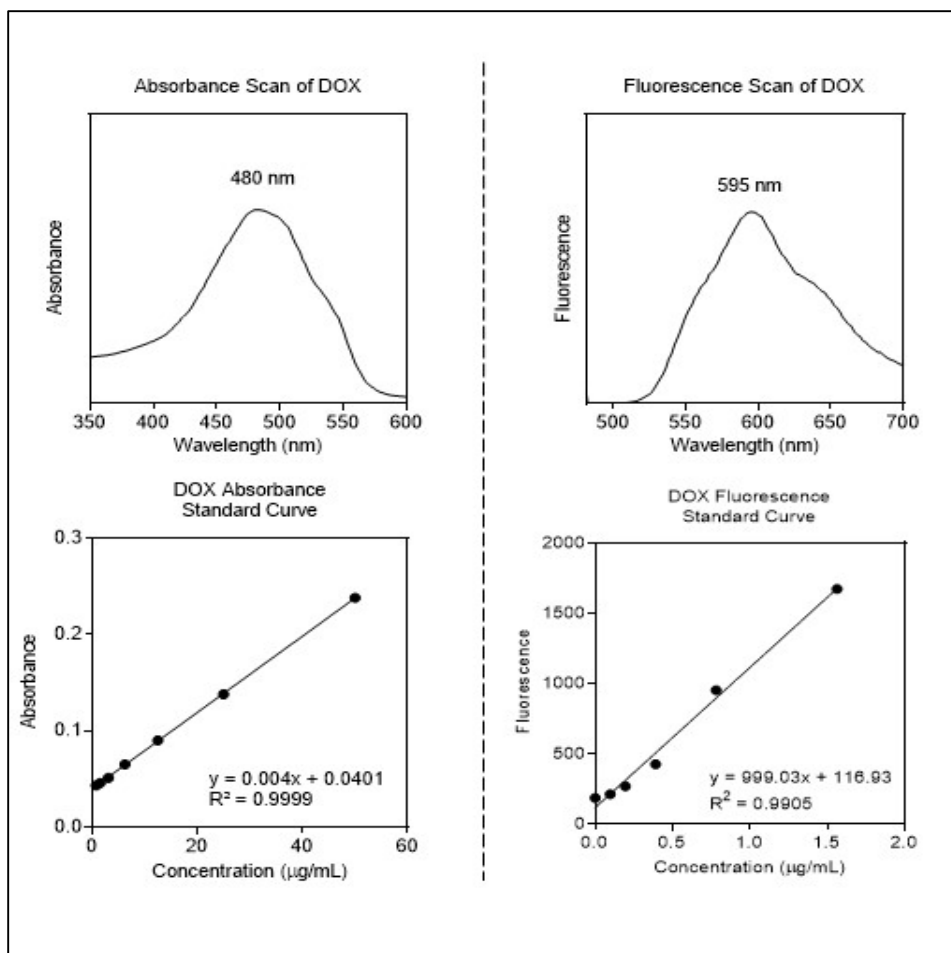


**Figure 6 – Plate reader calibration curves for DOX. Both absorbance and fluorescence had standard curves with  $R^2 > 0.99$ , for accurate conversion of these values to their equivalence in  $\mu\text{g/mL}$  of DOX.**



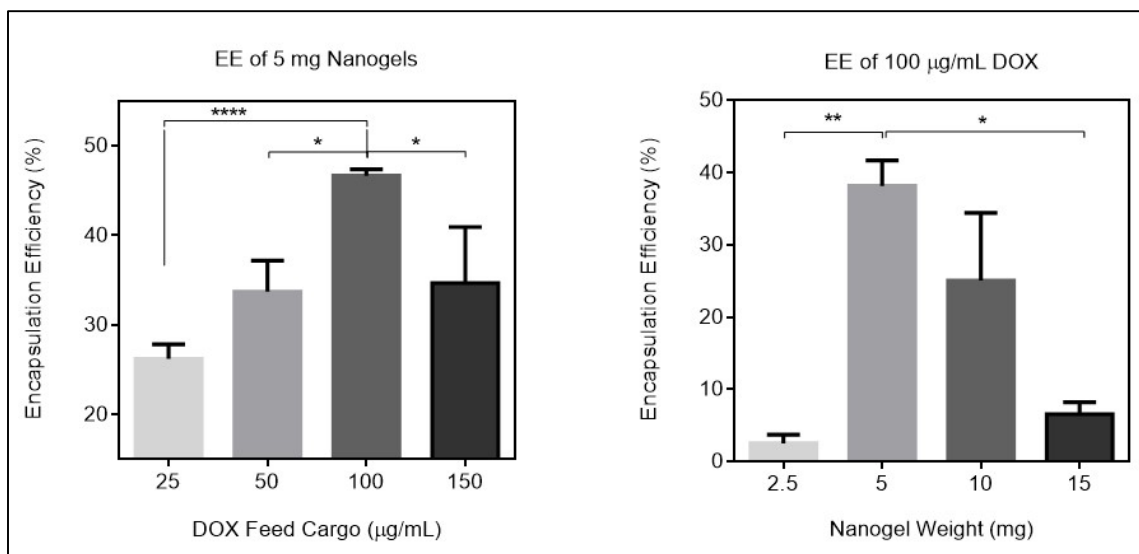


**Figure 7 – Encapsulation efficiency results. EE studies on 5 mg nanogels with various DOX solutions and on various nanogel weights with 100 µg/mL DOX solutions.**

After six hours of exposure to a heated environment above the transition temperature of the nanogels,  $74.6 \pm 6.3\%$  of encapsulated DOX was released (**Figure 8a**). For the experiments run at 37 C, release was limited to less than 25%. Comparable studies showed similar behavior in release kinetics. [68] This limited release could be due to surface adhered DOX not fully within the nanogel, or due to a slight decrease in hydrodynamic diameter at 37 C, which was seen via DLS temperature sweep at the beginning of the transition temperature range quantified in **Figure 3c**. However, with a plateau after this burst release and the low concentration released from the nanogels, we opted to continue using our synthesized nanogels for future experiments. The significantly enhanced release ( $p < 0.01$ ) at a higher temperature, particularly above VPTT, confirmed the temperature-triggered behavior of the PNIPAM-co-AM shell of the nanogel.

An average of 75.1% of the loaded DOX was released from our nanocomposite into the PBS bath after 24 hours of thermal exposure above the VPTT (50 C) (**Figure 8b**). A significantly lower ( $p < 0.05$ ) release amount was shown from the 37 C exposed samples. Significantly enhanced release in a thermally-triggered environment showed that the fixity of the gel slowed release, but a large percentage was still released into the environment after a short time range. This delay in release is shown in many papers that utilize macroscopic gel matrices for drug release studies. [69]

An average release of  $23.4 \pm 1.4\%$  was shown after 1 hour of exposure to the AMF, and in the same environmental conditions with no AMF-exposure, a smaller burst release of 7.8% was observed (**Figure 8c**). Release after AMF exposure was lower than similar results by Jaiswal *et al* (~40%), but this is expected to be due to slower diffusion from the highly crosslinked gel. [45] Also, our induction heating system had a lower frequency of 170 kHz than Jaiswal's experiments (230 kHz) due to limitations in our system. It is also worth noting that the field strength utilized for this experiment (0.0375 T) were lower than the AMF strength found in commercial MRIs (0.05 to 3 T), so exposure to a larger field would improve our release speed.

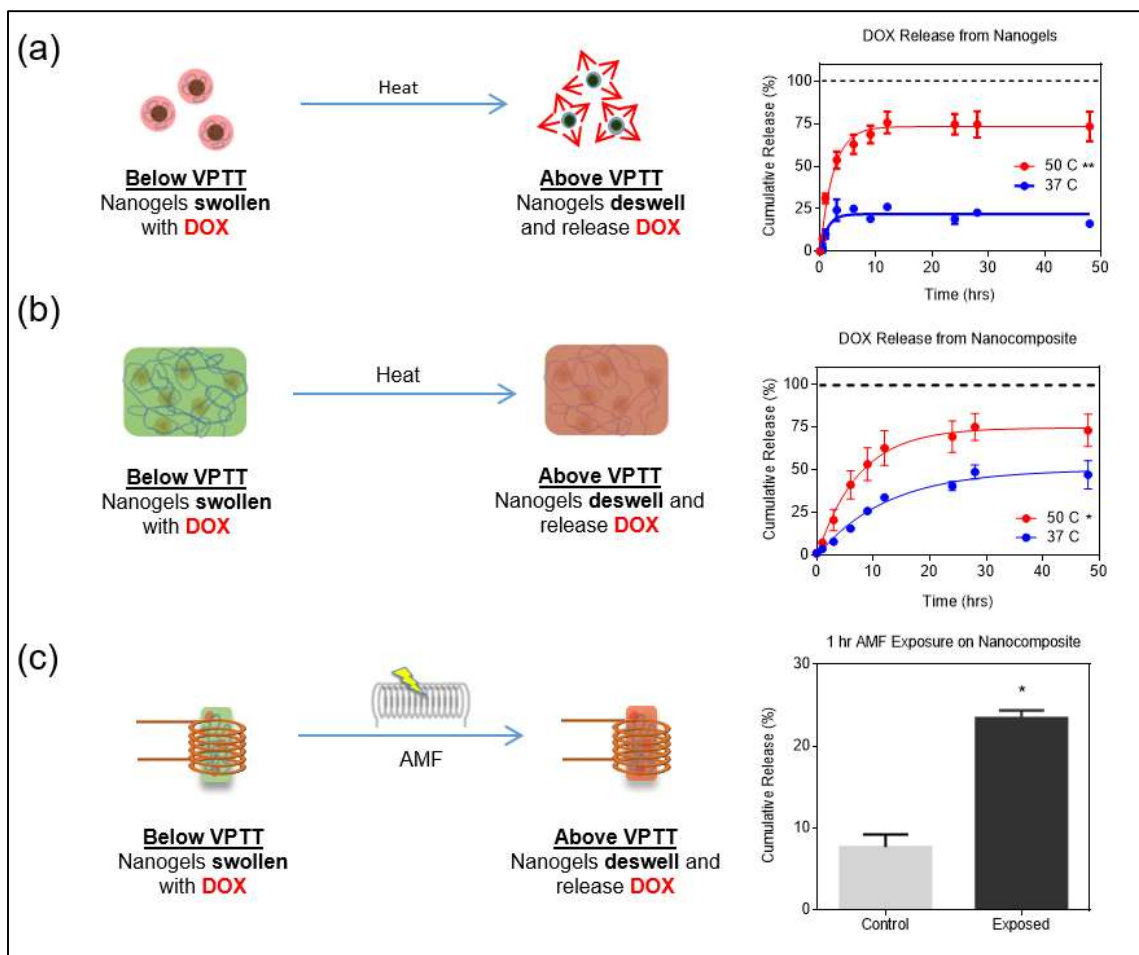


**Figure 8 - Release studies on nanogels and nanocomposites. (a) Release kinetics from nanogels were shown to be significantly different ( $p < 0.01$ ) when exposed to temperatures above the VPTT. (b) Release from nanocomposite also showed significant difference ( $p < 0.05$ ) when exposed to temperatures above VPTT. (c) Nanocomposite was exposed to an AMF at RT for 1 hour and shown to be significantly greater than nanocomposites with no magnetic field exposure.**

A significant difference ( $p < 0.0001$ ) was shown when comparing cumulative release after 1 hour for AMF-exposed samples versus thermally exposed samples (**Figure 9**). An improved release after 1 hour with magnetic exposure suggests a potentially enhanced release profile for our magnetically-responsive nanocomposite. Similar observations have been made by other researchers such as Liu *et al.* in which a significant

difference between magnetic and thermal release was shown from their nanogel system. [70] In their work, they showed a more pronounced burst release from their magnetically-triggered nanogels than their thermally-triggered nanogels. Temperature radiated due to magnetic hyperthermia could not be evaluated with thermocouple or IR camera due to the small weight percentage of magnetic nanoparticles within a low amount of loaded nanogels. We believe that this enhanced release could be due to delays in thermal balance in our PBS bath studies that potentially delayed the burst releases above the VPTT. Based off our data, a triggered release could be observed with magnetic fields in addition to temperatures above body temperature. These results proved that our system can be utilized for biomedical purposes.

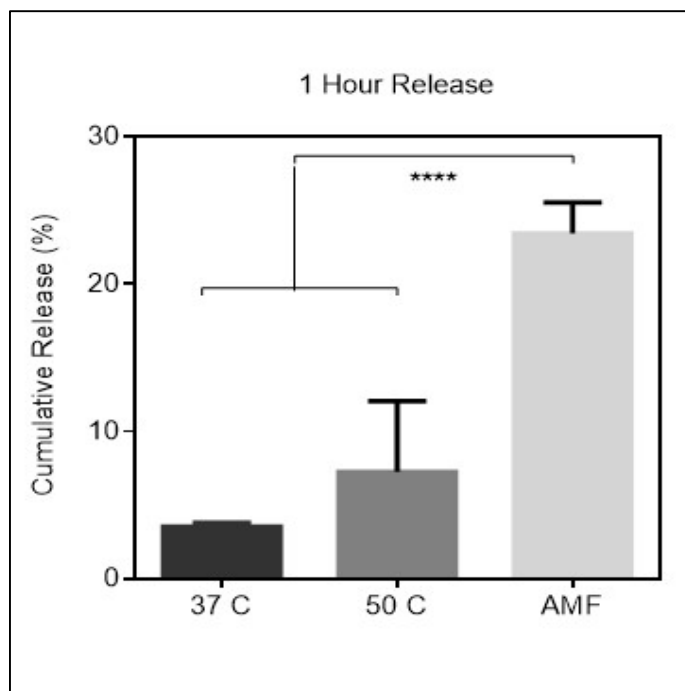


**Figure 9 – 1 hour release comparison. Nanocomposite cumulative release at 1 hour of temperature (37 C, 50 C) and 1 hour of AMF exposure (AMF) showed significant difference ( $p < 0.0001$ ) between thermal and magnetic releases.**

### III.4 2D Cell Viability

Based off the results from **Figure 8a**, the “Free DOX” weight chosen was 30  $\mu\text{g}$  (or  $\sim 75\%$  of our average EE of 42.1  $\mu\text{g}$ ) per 1 mL. With this concentration, cell viability decreased to approximately  $17.7 \pm 2.5\%$  of normalized mitochondrial activity. Doxorubicin works as an anti-cancer drug by entering the nucleus and intercalating with DNA to stop DNA replication and ultimately causes cytostasis. [2] Therefore, free DOX exposure on fast-replicating cell types like MOS-J and MC3T3 lines cause significant cell death.

To evaluate the viability of the delivery system, *in vitro* studies utilizing preosteoblasts and osteosarcomas were conducted. First, the IC<sub>50</sub> of DOX used to treat the osteosarcoma cells was determined to be above 10 µg/mL so a concentration of 30 µg/mL was acceptable for the remainder of the experiments (**Figure 10**). RFP-MOSJ cells were treated with free DOX, nanogels, DOX-loaded nanogels, gel, and Dox-loaded nanocomposites for 6 hours. After 48 hours, live/dead staining showed qualitatively that while free DOX caused significant cell death, exposure to nanogels and DOX-loaded nanogels maintained cell viability (**Figures 11a, 12a**). MTT assays quantified that the solutions of free DOX significantly ( $p < 0.0001$ ) reduced preosteoblast and osteosarcoma viability in comparison to the DOX-loaded nanogels and nanocomposites (**Figures 11b, 12b**).

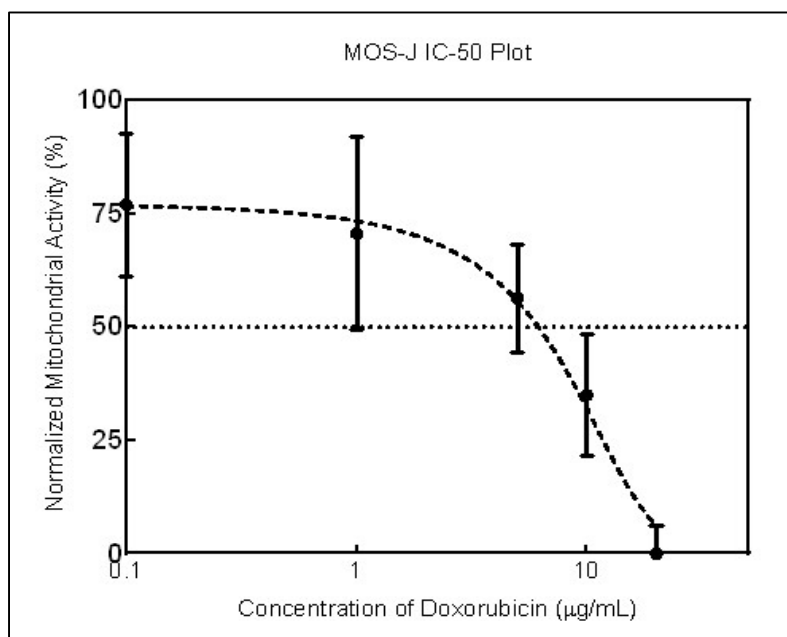


**Figure 10 – MOS-J IC-50 plot. IC-50 curve for MOS-J cell line when exposed to varying concentrations of DOX. Concentrations above 10 µg/mL DOX were sufficient for killing over 50% of these cells.**

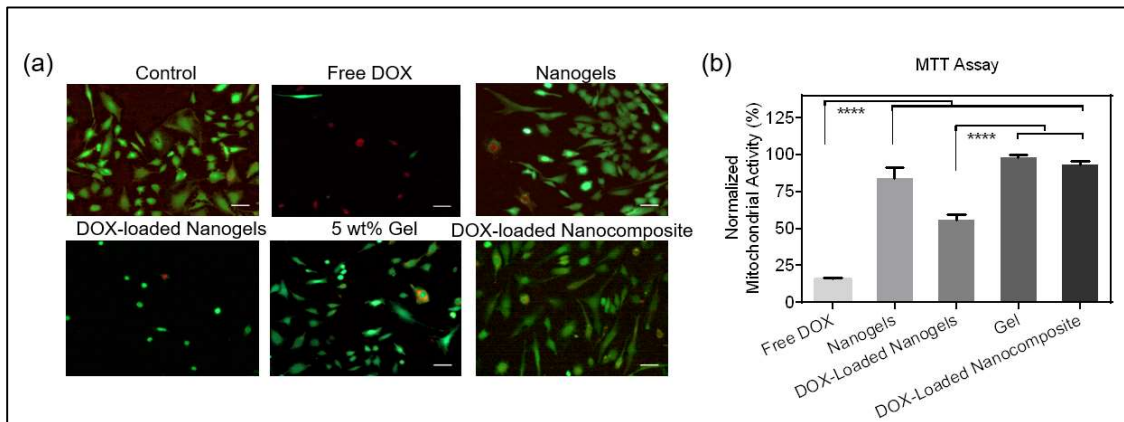


**Figure 11 – Mouse osteosarcoma (MOS-J) cell line exposure studies. (a) Live/Dead staining of MOS-Js showed viability of all components of the nanocomposite in comparison to a solution of DOX (Free DOX). (b) Quantifiable viability was gathered via MTT assays. A significant difference ( $p < 0.0001$ ) was shown between free DOX and all other samples. DOX-loaded nanogels also showed the same significant difference with gel and DOX-loaded nanocomposites.**

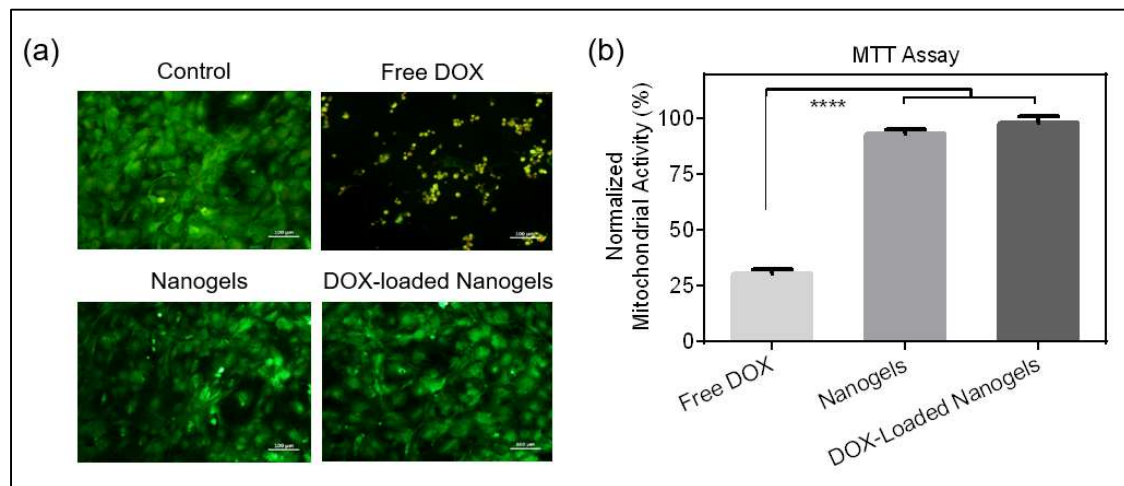


**Figure 12 – Mouse preosteoblast (MC3T3) cell line exposure studies. (a) Live/Dead staining of MC3T3s showed viability of all components of the nanocomposite in comparison to a solution of DOX (Free DOX). (b) Quantifiable viability was gathered via MTT assays. A significant difference ( $p < 0.0001$ ) was shown between free DOX and all other samples.**

When comparing between the two cell types, viability was shown to be lower on average for MOS-J cells exposed to DOX-loaded nanogels than for the same sample type exposed to MC3T3 cells (**Figure 13**). This is in line with work by Maiorano *et al.*, who explored the effects of viability on two cell types grown with different media that uptake the same amount and type of nanoparticles. [71] There is also the chance that some DOX was adhered to the surface instead of loaded fully within the nanogels. However, by suspending and fixating the nanogels within the gel matrix, we have shown that we can prevent this viability difference while still releasing DOX. Exposure of the DOX-loaded nanocomposite to MOS-J cells maintained viability in contrast to the DOX loaded nanogels ( $p < 0.0001$ ).

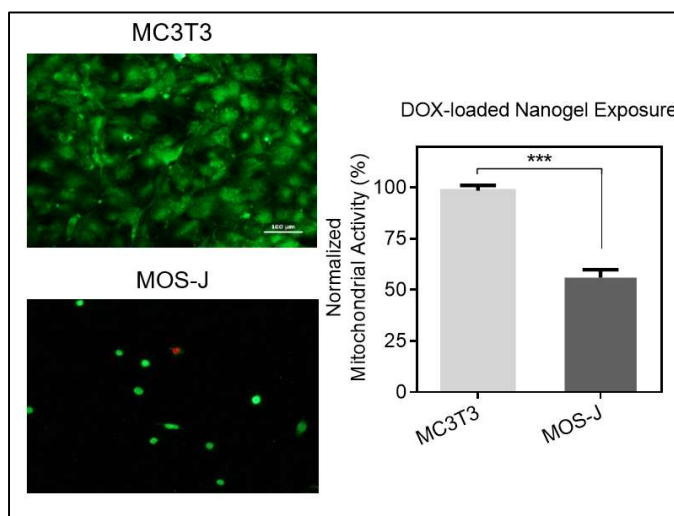


**Figure 13 – Dox-loaded nanogel comparison. Comparison of DOX-loaded nanogel effects on MC3T3 and MOS-J cells showed a significant difference ( $p < 0.001$ ) between the two cell types.**



#### IV. CONCLUSIONS

To develop a new drug delivery construct, PNIPAM-co-AM/MNP nanogels were synthesized and characterized to be functional and controlled in a regulated manner. It has been shown that we can synthesize citric acid-coated  $\text{Fe}_3\text{O}_4$  nanoparticles, have them encapsulated by a thermoresponsive copolymer of PNIPAM-co-AM with a VPTT behavior of around 45 C. With these nanogels, we were able to show a large burst release of Doxorubicin at a temperature higher than the VPTT, and very limited release under this temperature. When these nanogels were exposed to healthy and cancerous cells, we showed that cells remained highly viable, thus showing controllability of release at body temperature. We were also able to show that these nanogels can release DOX into surrounding cells even after incorporation into a crosslinked gelatin-based hydrogel. Although the construct would only be injected into already existing or excised tumor sites, if any of the drug-loaded nanogels come loose due to simple physical fixation, the localized external application of AMF is hypothesized to prevent release from elsewhere in the body. In order to mitigate this possibility, nanogels could be functionalized and chemically attached to the macroscopic gel. Finally, our nanocomposite was exposed to an AMF like one presented by an MRI and a preliminary study showed a distinct increase in DOX release versus a nanocomposite not exposed to an AMF.

In the future, looking at changing AMF intensity and frequency and increasing sample size would be beneficial to optimizing drug delivery out of the already implanted construct. Commercial MRIs found in many patient hospitals produce a field strength

ranging from 0.05 to 3 T. Our calculations showed that we were below this range, which allows the ability for us to continue working under the premise that this nanocomposite will work for biomedical applications and gives us the potential to expose the nanocomposite construct with a higher field for faster release. Collaboration with a laboratory or clinic with an MRI machine would allow us to compare the results from our induction heating system with a commercial standard in providing external magnetic stimuli process to get maximal drug delivery from our construct.

Although addition of 5 mg nanogel to the 1 mL solution of 5 wt% gel showed no true difference in rheological characteristics, It is well documented that addition of nanoparticles alters these properties, so future studies would be done in order to test optimal release profiles in a more realistic tumor model where more cells would be present and release from a larger system would vary. [52] Therefore, altering weights of nanogels exposed to cells and altering number of cells can give us a better picture of the amount of nanogels required to have sufficient coverage of a quantifiable tissue area.

We also recognize that this drug delivery system limits our potential market size to those without metallic implants due to the risks that an AMF has on metallic compounds. However, we feel that the market is sizeable enough that this gives us a decent entry point if this construct is pushed forward to further testing for market approval. A full market analysis of patients that this construct can help can also be performed in the future if needed. Instead of limiting our market to just patients with cancer, this nanocomposite construct can be loaded with any drug or combination of drugs to treat various medical

pathologies. Having potential to apply growth factors to this construct to regenerate tissue, we believe that this system could hold a future in the biomedical industry.

## REFERENCES

- [1] Society AC. Cancer Facts & Figures 2015. Atlanta, Ga: American Cancer Society; 2015.
- [2] Tacar O, Sriamornsak P, Dass CR. Doxorubicin: an update on anticancer molecular action, toxicity and novel drug delivery systems. *Journal of Pharmacy and Pharmacology*. 2013;65:157-70.
- [3] Bawa P, Pillay V, Choonara YE, du Toit LC. Stimuli-responsive polymers and their applications in drug delivery. *Biomed Mater*. 2009;4:15.
- [4] Zhao X, Ding X, Deng Z, Zheng Z, Peng Y, Long X. Thermoswitchable electronic properties of a gold nanoparticle/hydrogel composite. *Macromolecular Rapid Communications*. 2005;26:1784-7.
- [5] De SK, Aluru NR, Johnson B, Crone WC, Beebe DJ, Moore J. Equilibrium swelling and kinetics of pH-responsive hydrogels: Models, experiments, and simulations. *J Microelectromech Syst*. 2002;11:544-55.
- [6] Kwok CS, Mourad PD, Crum LA, Ratner BD. Self-assembled molecular structures as ultrasonically-responsive barrier membranes for pulsatile drug delivery. *J Biomed Mater Res*. 2001;57:151-64.
- [7] Klouda L, Mikos AG. Thermoresponsive hydrogels in biomedical applications. *European Journal of Pharmaceutics and Biopharmaceutics*. 2008;68:34-45.
- [8] Guardia P, Di Corato R, Lartigue L, Wilhelm C, Espinosa A, Garcia-Hernandez M, et al. Water-soluble iron oxide nanocubes with high values of specific absorption rate for cancer cell hyperthermia treatment. *ACS Nano*. 2012;6:3080-91.
- [9] Lu A-H, Salabas EL, Schüth F. Magnetic nanoparticles: synthesis, protection, functionalization, and application. *Angewandte Chemie International Edition*. 2007;46:1222-44.
- [10] Wang YX. Superparamagnetic iron oxide based MRI contrast agents: current status of clinical application. *Quantitative Imaging in Medicine and Surgery*. 2011;1:35-40.
- [11] Hayashi K, Nakamura M, Sakamoto W, Yogo T, Miki H, Ozaki S, et al. Superparamagnetic nanoparticle clusters for cancer theranostics combining magnetic resonance imaging and hyperthermia treatment. *Theranostics*. 2013;3:366-76.

- [12] Kim JI, Lee BS, Chun C, Cho J-K, Kim S-Y, Song S-C. Long-term theranostic hydrogel system for solid tumors. *Biomaterials*. 2012;33:2251-9.
- [13] Georgiadou V, Kokotidou C, Le Droumaguet B, Carbonnier B, Choli-Papadopoulou T, Dendrinou-Samara C. Oleylamine as a beneficial agent for the synthesis of CoFe<sub>2</sub>O<sub>4</sub> nanoparticles with potential biomedical uses. *Dalton Transactions*. 2014;43:6377-88.
- [14] Sun SH, Zeng H, Robinson DB, Raoux S, Rice PM, Wang SX, et al. Monodisperse MFe<sub>2</sub>O<sub>4</sub> (M = Fe, Co, Mn) nanoparticles. *Journal of the American Chemical Society*. 2004;126:273-9.
- [15] Hariri G, Wellons MS, Morris WH, 3rd, Lukehart CM, Hallahan DE. Multifunctional FePt nanoparticles for radiation-guided targeting and imaging of cancer. *Annals of biomedical engineering*. 2011;39:946-52.
- [16] Maiti D, Saha A, Devi PS. Surface modified multifunctional ZnFe<sub>2</sub>O<sub>4</sub> nanoparticles for hydrophobic and hydrophilic anti-cancer drug molecule loading. *Physical Chemistry Chemical Physics*. 2016;18:1439-50.
- [17] Manukyan KV, Chen Y-S, Rouvimov S, Li P, Li X, Dong S, et al. Ultrasmall  $\alpha$ -Fe<sub>2</sub>O<sub>3</sub> superparamagnetic nanoparticles with high magnetization prepared by template-assisted combustion process. *The Journal of Physical Chemistry C*. 2014;118:16264-71.
- [18] Subhankar B, Wolfgang K. Supermagnetism. *Journal of Physics D: Applied Physics*. 2009;42:013001.
- [19] Gupta AK, Gupta M. Synthesis and surface engineering of iron oxide nanoparticles for biomedical applications. *Biomaterials*. 2005;26:3995-4021.
- [20] Ghosh S, Kumar SRP, Puri IK, Elankumaran S. Magnetic assembly of 3D cell clusters: visualizing the formation of an engineered tissue. *Cell Prolif*. 2016;49:134-44.
- [21] Tang M, Wang Q, Jiang M, Xu L, Shi Z-G, Zhang T, et al. Magnetic solid-phase extraction based on methylcellulose coated-Fe<sub>3</sub>O<sub>4</sub>-SiO<sub>2</sub>-phenyl for HPLC-DAD analysis of sildenafil and its metabolite in biological samples. *Talanta*. 2014;130:427-32.
- [22] Kılınç E. Fullerene C<sub>60</sub> functionalized  $\gamma$ -Fe<sub>2</sub>O<sub>3</sub> magnetic nanoparticle: Synthesis, characterization, and biomedical applications. *Artificial Cells, Nanomedicine, and Biotechnology*. 2016;44:298-304.
- [23] Mroz P, Pawlak A, Satti M, Lee H, Wharton T, Gali H, et al. Functionalized fullerenes mediate photodynamic killing of cancer cells: Type I versus Type II photochemical mechanism. *Free Radical Biology and Medicine*. 2007;43:711-9.

- [24] Tóth É, Bolskar RD, Borel A, González G, Helm L, Merbach AE, et al. Water-soluble gadofullerenes: toward high-relaxivity, pH-responsive MRI contrast agents. *Journal of the American Chemical Society*. 2005;127:799-805.
- [25] Chen C-L, Kuo L-R, Lee S-Y, Hwu Y-K, Chou S-W, Chen C-C, et al. Photothermal cancer therapy via femtosecond-laser-excited FePt nanoparticles. *Biomaterials*. 2013;34:1128-34.
- [26] Sahu NK, Gupta J, Bahadur D. PEGylated FePt-Fe<sub>3</sub>O<sub>4</sub> composite nanoassemblies (CNAs): in vitro hyperthermia, drug delivery and generation of reactive oxygen species (ROS). *Dalton transactions (Cambridge, England : 2003)*. 2015;44:9103-13.
- [27] Salunkhe AB, Khot VM, Thorat ND, Phadatare MR, Sathish CI, Dhawale DS, et al. Polyvinyl alcohol functionalized cobalt ferrite nanoparticles for biomedical applications. *Appl Surf Sci*. 2013;264:598-604.
- [28] Kim JI, Chun C, Kim B, Hong JM, Cho J-K, Lee SH, et al. Thermosensitive/magnetic poly(organophosphazene) hydrogel as a long-term magnetic resonance contrast platform. *Biomaterials*. 2012;33:218-24.
- [29] Barrena R, Casals E, Colón J, Font X, Sánchez A, Puntès V. Evaluation of the ecotoxicity of model nanoparticles. *Chemosphere*. 2009;75:850-7.
- [30] Karlsson HL, Gustafsson J, Cronholm P, Möller L. Size-dependent toxicity of metal oxide particles—A comparison between nano- and micrometer size. *Toxicology Letters*. 2009;188:112-8.
- [31] Jaiswal MK, Mehta S, Banerjee R, Bahadur D. A comparative study on thermoresponsive magnetic nanohydrogels: role of surface-engineered magnetic nanoparticles. *Colloid and Polymer Science*. 2011;290:607-17.
- [32] Han HD, Shin BC, Choi HS. Doxorubicin-encapsulated thermosensitive liposomes modified with poly(N-isopropylacrylamide-co-acrylamide): Drug release behavior and stability in the presence of serum. *European Journal of Pharmaceutics and Biopharmaceutics*. 2006;62:110-6.
- [33] Lo C-L, Lin K-M, Hsiue G-H. Preparation and characterization of intelligent core-shell nanoparticles based on poly(D,L-lactide)-g-poly(N-isopropyl acrylamide-co-methacrylic acid). *Journal of Controlled Release*. 2005;104:477-88.
- [34] Li Z, Shen J, Ma H, Lu X, Shi M, Li N, et al. Preparation and characterization of sodium alginate/poly(N-isopropylacrylamide)/clay semi-IPN magnetic hydrogels. *Polymer Bulletin*. 2011;68:1153-69.

- [35] Gant RM, Abraham AA, Hou Y, Cummins BM, Grunlan MA, Côté GL. Design of a self-cleaning thermoresponsive nanocomposite hydrogel membrane for implantable biosensors. *Acta Biomaterialia*. 2010;6:2903-10.
- [36] Baeza A, Guisasola E, Ruiz-Hernández E, Vallet-Regí M. Magnetically triggered multidrug release by hybrid mesoporous silica nanoparticles. *Chemistry of Materials*. 2012;24:517-24.
- [37] Sivakumaran D, Maitland D, Hoare T. Injectable microgel-hydrogel composites for prolonged small-molecule drug delivery. *Biomacromolecules*. 2011;12:4112-20.
- [38] Tan H, Ramirez CM, Miljkovic N, Li H, Rubin JP, Marra KG. Thermosensitive injectable hyaluronic acid hydrogel for adipose tissue engineering. *Biomaterials*. 2009;30:6844-53.
- [39] Yang J, Yamato M, Shimizu T, Sekine H, Ohashi K, Kanzaki M, et al. Reconstruction of functional tissues with cell sheet engineering. *Biomaterials*. 2007;28:5033-43.
- [40] Hong SW, Kim DY, Lee JU, Jo WH. Synthesis of polymeric temperature sensor based on photophysical property of fullerene and thermal sensitivity of poly(N-isopropylacrylamide). *Macromolecules*. 2009;42:2756-61.
- [41] Yang C-C, Tian Y, Jen AKY, Chen W-C. New environmentally responsive fluorescent N-isopropylacrylamide copolymer and its application to DNA sensing. *Journal of Polymer Science Part A: Polymer Chemistry*. 2006;44:5495-504.
- [42] Wang N, Guan YP, Yang LR, Jia LW, Wei XT, Liu HZ, et al. Magnetic nanoparticles (MNPs) covalently coated by PEO-PPO-PEO block copolymer for drug delivery. *Journal of Colloid and Interface Science*. 2013;395:50-7.
- [43] Valverde-Aguilar G, Pérez-Mazariego J, Marquina V, Gómez R, Aguilar-Franco M, Garcia-Macedo J. Effect of PEO-PPO-PEO triblock copolymers in the synthesis of magnetic nanoparticles embedded in SiO and TiO matrices by sol-gel method. *Journal of Materials Science*. 2015;50:704-16.
- [44] Kang GD, Cheon SH, Song SC. Controlled release of doxorubicin from thermosensitive poly(organophosphazene) hydrogels. *International journal of pharmaceutics*. 2006;319:29-36.
- [45] Jaiswal MK, De M, Chou SS, Vasavada S, Bleher R, Prasad PV, et al. Thermoresponsive magnetic hydrogels as theranostic nanoconstructs. *ACS Applied Materials & Interfaces*. 2014;6:6237-47.

- [46] Principles of cancer therapy: surgery. In: Mark H. Beers M, Robert Berkow M, editors. The Merck Manual of Diagnosis and Therapy. Whitehouse Station, NJ: Merck Research Laboratories; 1999.
- [47] Hayashi K, Nakamura M, Sakamoto W, Yogo T, Miki H, Ozaki S, et al. Superparamagnetic nanoparticle clusters for cancer theranostics combining magnetic resonance imaging and hyperthermia treatment. *Theranostics*. 2013;3:366-76.
- [48] Hayashi K, Nakamura M, Miki H, Ozaki S, Abe M, Matsumoto T, et al. Magnetically responsive smart nanoparticles for cancer treatment with a combination of magnetic hyperthermia and remote-control drug release. *Theranostics*. 2014;4:834-44.
- [49] Schultz N. Leaker tumor vessels enhance drug delivery. *MIT Technology Review* 2010. p. 2.
- [50] McDonald DM, Baluk P. Significance of blood vessel leakiness in cancer. *Cancer research*. 2002;62:5381-5.
- [51] Weissleder R, Stark DD, Engelstad BL, Bacon BR, Compton CC, White DL, et al. Superparamagnetic iron oxide: pharmacokinetics and toxicity. *AJR American journal of roentgenology*. 1989;152:167-73.
- [52] Gaharwar AK, Avery RK, Assmann A, Paul A, McKinley GH, Khademhosseini A, et al. Shear-thinning nanocomposite hydrogels for the treatment of hemorrhage. *ACS Nano*. 2014;8:9833-42.
- [53] Van Den Bulcke AI, Bogdanov B, De Rooze N, Schacht EH, Cornelissen M, Berghmans H. Structural and rheological properties of methacrylamide modified gelatin hydrogels. *Biomacromolecules*. 2000;1:31-8.
- [54] Nichol JW, Koshy ST, Bae H, Hwang CM, Yamanlar S, Khademhosseini A. Cell-laden microengineered gelatin methacrylate hydrogels. *Biomaterials*. 2010;31:5536-44.
- [55] Koshy ST, Desai RM, Joly P, Li JY, Bagrodia RK, Lewin SA, et al. Click-crosslinked injectable gelatin hydrogels. *Adv Healthc Mater*. 2016;5:541-7.
- [56] Loessner D, Meinert C, Kaemmerer E, Martine LC, Yue K, Levett PA, et al. Functionalization, preparation and use of cell-laden gelatin methacryloyl-based hydrogels as modular tissue culture platforms. *Nat Protoc*. 2016;11:727-46.
- [57] Chilkoti A, Dreher MR, Meyer DE, Raucher D. Targeted drug delivery by thermally responsive polymers. *Advanced Drug Delivery Reviews*. 2002;54:613-30.



- [58] Nigam S, Barick KC, Bahadur D. Development of citrate-stabilized Fe<sub>3</sub>O<sub>4</sub> nanoparticles: Conjugation and release of doxorubicin for therapeutic applications. *Journal of Magnetism and Magnetic Materials*. 2011;323:237-43.
- [59] Zhang J, Chen H, Xu L, Gu Y. The targeted behavior of thermally responsive nanohydrogel evaluated by NIR system in mouse model. *Journal of Controlled Release*. 2008;131:34-40.
- [60] Fairbanks BD, Schwartz MP, Bowman CN, Anseth KS. Photoinitiated polymerization of PEG-diacrylate with lithium phenyl-2,4,6-trimethylbenzoylphosphinate: polymerization rate and cytocompatibility. *Biomaterials*. 2009;30:6702-7.
- [61] Rudnev V. *Handbook of induction heating*. New York :: Marcel Dekker; 2003.
- [62] Legendre JY, Szoka FC. Delivery of plasmid dna into mammalian-cell lines using ph-sensitive liposomes - comparison with cationic liposomes. *Pharm Res*. 1992;9:1235-42.
- [63] Lee RJ, Low PS. Folate-mediated tumor cell targeting of liposome-entrapped doxorubicin in vitro. *Biochimica et Biophysica Acta (BBA) - Biomembranes*. 1995;1233:134-44.
- [64] Constantin M, Cristea M, Ascenzi P, Fundueanu G. Lower critical solution temperature versus volume phase transition temperature in thermoresponsive drug delivery systems. *Express Polym Lett*. 2011;5:839-48.
- [65] Paul A, Hasan A, Kindi HA, Gaharwar AK, Rao VT, Nikkhah M, et al. Injectable graphene oxide/hydrogel-based angiogenic gene delivery system for vasculogenesis and cardiac repair. *ACS Nano*. 2014;8:8050-62.
- [66] Monteux C, Mangeret R, Laibe G, Freyssingeas E, Bergeron V, Fuller G. Shear surface rheology of poly(N-isopropylacrylamide) adsorbed layers at the air–water interface. *Macromolecules*. 2006;39:3408-14.
- [67] Mason BN, Califano JP, Reinhart-King CA. Matrix stiffness: a regulator of cellular behavior and tissue formation. In: Bhatia KS, editor. *Engineering Biomaterials for Regenerative Medicine: Novel Technologies for Clinical Applications*. New York, NY: Springer New York; 2012. p. 19-37.
- [68] Shah SA, Asdi MH, Hashmi MU, Umar MF, Awan S-U. Thermo-responsive copolymer coated MnFe<sub>2</sub>O<sub>4</sub> magnetic nanoparticles for hyperthermia therapy and controlled drug delivery. *Materials Chemistry and Physics*. 2012;137:365-71.

[69] Dong Z, Wang Q, Du Y. Alginate/gelatin blend films and their properties for drug controlled release. *Journal of Membrane Science*. 2006;280:37-44.

[70] Liu TY, Hu SH, Liu KH, Shaiu RS, Liu DM, Chen SY. Instantaneous drug delivery of magnetic/thermally sensitive nanospheres by a high-frequency magnetic field. *Langmuir*. 2008;24:13306-11.

[71] Maiorano G, Sabella S, Sorce B, Brunetti V, Malvindi MA, Cingolani R, et al. Effects of cell culture media on the dynamic formation of protein–nanoparticle complexes and influence on the cellular response. *ACS Nano*. 2010;4:7481-91.